

## Structural Aspects for Evolution of $\beta$ -Lactamases from Penicillin-Binding Proteins

Samy O. Meroueh,<sup>†,||</sup> George Minasov,<sup>‡,||</sup> Wenlin Lee,<sup>†</sup> Brian K. Shoichet,<sup>§</sup> and Shahriar Mobashery<sup>\*,†</sup>

Contribution from the Department of Chemistry and Biochemistry, University of Notre Dame, Notre Dame, Indiana 46556, Department of Molecular Pharmacology and Biological Chemistry, Northwestern University, 303 East Chicago Avenue, Chicago, Illinois 60611, and Department of Pharmaceutical Chemistry, University of California, San Francisco, Genentech Hall, San Francisco, California 94143

Received February 25, 2003; E-mail: mobashery@nd.edu

**Abstract:** Penicillin-binding proteins (PBPs), biosynthetic enzymes of bacterial cell wall assembly, and  $\beta$ -lactamases, resistance enzymes to  $\beta$ -lactam antibiotics, are related to each other from an evolutionary point of view. Massova and Mobashery (*Antimicrob. Agents Chemother.* **1998**, *42*, 1–17) have proposed that for  $\beta$ -lactamases to have become effective at their function as antibiotic resistance enzymes, they would have had to undergo structure alterations such that they would not interact with the peptidoglycan, which is the substrate for PBPs. A cephalosporin analogue, 7 $\beta$ -[N-Acetyl-L-alanyl- $\gamma$ -D-glutamyl-L-lysine]-3-acetoxymethyl-3-cephem-carboxylic acid (compound **6**), was conceived and synthesized to test this notion. The X-ray structure of the complex of this cephalosporin bound to the active site of the deacylation-deficient Q120L/Y150E variant of the class C AmpC  $\beta$ -lactamase from *Escherichia coli* was solved at 1.71 Å resolution. This complex revealed that the surface for interaction with the strand of peptidoglycan that acylates the active site, which is present in PBPs, is absent in the  $\beta$ -lactamase active site. Furthermore, insertion of a peptide in the  $\beta$ -lactamase active site at a location where the second strand of peptidoglycan in some PBPs binds has effectively abolished the possibility for such interaction with the  $\beta$ -lactamase. A 2.6 ns dynamics simulation was carried out for the complex, which revealed that the peptidoglycan surrogate (i.e., the active-site-bound ligand) undergoes substantial motion and is not stabilized for binding within the active site. These factors taken together disclose the set of structure modifications in the antibiotic resistance enzyme that prevent it from interacting with the peptidoglycan, en route to achieving catalytic proficiency for their intended function.

Sequence similarity, a shared protein fold, conservation of structural motifs, and mechanistic features such as active site acylation by their respective substrates at specific serine residues have been proposed as consistent with kinship of  $\beta$ -lactamases and penicillin-binding proteins (PBPs).<sup>1–4</sup>  $\beta$ -Lactamases are bacterial resistance enzymes to  $\beta$ -lactam antibiotics, and PBPs are biosynthetic enzymes involved in assembly and processing of the cell wall. It is clear that, despite the divergence of the sequences, the general protein fold for these families of enzymes is preserved. The divergence of the sequences has allowed for impressive diversification of function among these proteins.

It is widely thought that the genes for the more ancient PBPs gave rise to those of  $\beta$ -lactamases.<sup>2,4–6</sup> PBPs process the building blocks for the cell wall, namely the peptidoglycan (**1**). Two of the important PBP activities are the DD-transpeptidase and DD-peptidase reactions. The former activity is responsible for the final step of cell wall assembly by cross-linking two strands of peptidoglycan (species **4**). The latter activity removes the C-terminal D-alanine from the peptidoglycan (species **5**), a process that moderates the degree of cross-linking. The enzymes that carry out these activities catalyze their reactions in two steps that involve an intermediary acyl–enzyme species (**2**).

$\beta$ -Lactamases of classes A, C, and D also go through an acyl–enzyme species in their turnover of  $\beta$ -lactam antibiotics. These antibiotics mimic the structure of the acyl-D-Ala-D-Ala portion of the peptidoglycan.<sup>7</sup> However, the catalytic machiner-

<sup>†</sup> University of Notre Dame.

<sup>‡</sup> Northwestern University.

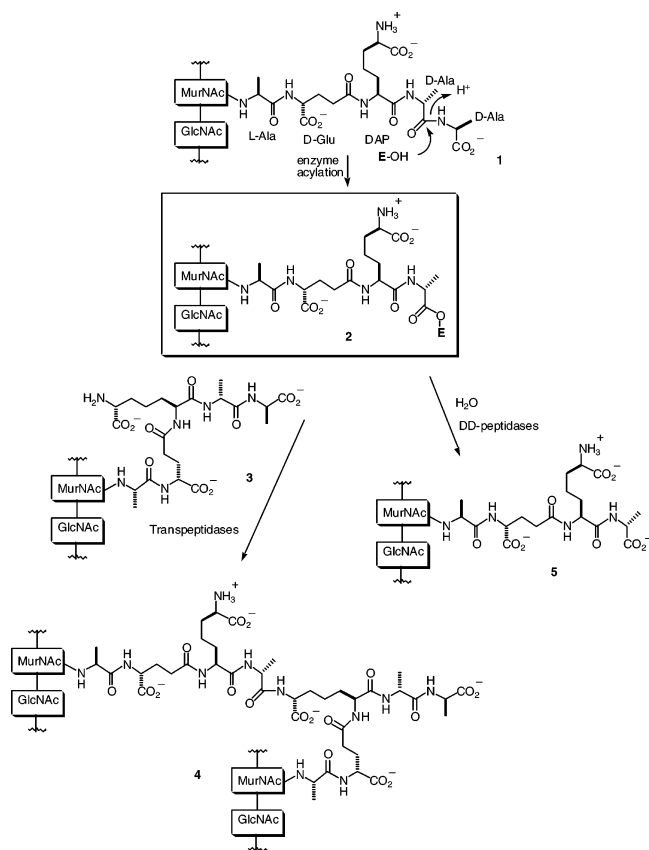
<sup>§</sup> University of California, San Francisco.

<sup>||</sup> These authors contributed equally.

- (1) Massova, I.; Mobashery, S. *Curr. Pharm. Des.* **1999**, *5*, 929–937.
- (2) Massova, I.; Mobashery, S. *Antimicrob. Agents Chemother.* **1998**, *42*, 1–17.
- (3) Kelly, J. A.; Dideberg, O.; Charlier, P.; Wery, J. P.; Libert, M.; Moews, P. C.; Knox, J. R.; Duez, C.; Fraipont, C.; Joris, B.; Dusart, J.; Frere, J. M.; Ghuysen, J. M. *Science* **1986**, *231*, 1429–1431.
- (4) Kotra, L. P.; Samama, J. P.; Mobashery, S. In *Bacterial Resistance to Antimicrobials, Mechanisms, Genetics, Medical Practice and Public Health*; Lewis, A., Salyers, A. A., Haber, H., Wax, R. G., Eds.; Marcel Dekker: 2002; p 123.

- (5) Ghuysen, J. M.; Charlier, P.; Coyette, J.; Duez, C.; Fonze, E.; Fraipont, C.; Goffin, C.; Joris, B.; Nguyen-Disteche, M. *Microb. Drug Resist.* **1996**, *2*, 163–175.
- (6) Ghuysen, J. M. *Annu. Rev. Microbiol.* **1991**, *45*, 37–67.
- (7) Tipper, D. J.; Strominger, J. L. *Proc. Natl. Acad. Sci. U.S.A.* **1965**, *54*, 1133–1141.

ies of these three classes of  $\beta$ -lactamases are distinct and have evolved independently from different ancestral PBP progenitors.<sup>2,4</sup>



$\beta$ -Lactamases have specialized as antibiotic resistance enzymes. Indeed, at least  $\beta$ -lactamases of classes A<sup>8</sup> and C<sup>9</sup> have fully evolved for their function by having become diffusion-limited for their preferred substrates. Massova and Mobashery have argued that for this catalytic proficiency to have reached its full potential,  $\beta$ -lactamases had to undergo alteration of their structures such that they would not bind to the peptidoglycan.<sup>2</sup> It was proposed based on the study of the existing X-ray structures for  $\beta$ -lactamases and PBPs that the corresponding surface of the PBP that would recognize the peptidoglycan strand that acylates the active site (present in both DD-transpeptidases and DD-peptidases) has been retracted in  $\beta$ -lactamases, such that molecular recognition of the peptidoglycan at this subsite of the active site would be impaired in  $\beta$ -lactamases. Furthermore, it was proposed that independent insertions of several amino acids in each of the cases of classes A and C of  $\beta$ -lactamases in the middle of the binding site for the second peptidoglycan strand (in the case of DD-transpeptidases) would abolish binding to the PBP substrate at this subsite. In the course of evolution of  $\beta$ -lactamases, the advent of these two sets of alterations in the structure of a given parental PBP would liberate the nascent  $\beta$ -lactamase from the interactions with the PBP substrate, facilitating its evolutionary trajectory toward the emergence of bona fide resistance enzymes.

In this report, we present results of X-ray crystallography of the class C  $\beta$ -lactamase from *Escherichia coli* bound to a

designed cephalosporin molecule that provides structural evidence for the proposal of Massova and Mobashery. Molecular dynamics simulations of this complex provide additional insights into these issues, suggesting that a portion of the ligand undergoes substantial motion in the active site of this enzyme in agreement with X-ray diffraction data, which revealed the existence of two possible conformers of the bound ligand. The 2.6 ns molecular dynamics simulation provided a detailed account of the motion of the ligand within the active site, which incidentally samples both conformers of the ligand seen within the X-ray structure of the complex.

## Experimental Procedures

Compound **14** was prepared by a literature method.<sup>10</sup> The Q120L/Y150E mutant of *E. coli* AmpC  $\beta$ -lactamase was made by oligonucleotide-directed mutagenesis, expressed, and purified as previously described.<sup>11</sup>

**N-Fluorenylmethoxycarbonyl-L-alanyl-D-glutamic Acid,  $\alpha$ -tert-Butyl,  $\gamma$ -Benzyl Diester (10).** To the mixture of *N*-Fmoc-L-alanine (**8**) (748 mg, 2.40 mmol), D-glutamic acid  $\alpha$ -tert-butyl- $\gamma$ -benzyl diester (**9**) (587 mg, 2.00 mmol), and HOBt (324 mg, 2.40 mmol) in CH<sub>2</sub>Cl<sub>2</sub> (20 mL) was added DCC (480 mg, 2.33 mmol). The resultant mixture was stirred at room temperature overnight. The precipitated DCU was filtered, and the filtrate was concentrated on a rotary evaporator. Ethyl acetate (30 mL) was added to the residue, and the suspension of additional DCU was filtered. The solvent was removed in vacuo, and the residue was redissolved in EtOAc. This solution was washed with 1 N HCl, water, sat. NaHCO<sub>3</sub>, water, and brine and then was dried over MgSO<sub>4</sub>. The solvent was removed in vacuo, and the product was purified by column chromatography (silica gel, 5:3 then 1:1 hexane/EtOAc) to give a white solid (761 mg, 65%). <sup>1</sup>H NMR (CDCl<sub>3</sub>):  $\delta$  1.39–1.43 (overlapping d and s, 12H), 1.91–2.05 (m, 1H), 2.18–2.27 (m, 1H), 2.35–2.51 (m, 2H), 4.20–4.23 (m, 1H), 4.32–4.39 (m, 3H), 4.50–4.55 (m, 1H), 5.10 (s, 2H), 5.61 (bd, 1H, *J* = 7.6 Hz), 6.94 (bd, 1H, *J* = 7.2 Hz), 7.28–7.40 (m, 9H), 7.58 (bd, 2H, *J* = 6.8 Hz), 7.75 (d, 2H, *J* = 8 Hz). <sup>13</sup>C NMR (CDCl<sub>3</sub>):  $\delta$  19.20, 27.67, 28.19, 30.45, 47.31, 50.72, 52.37, 66.77, 67.34, 82.79, 120.23, 125.37, 127.33, 127.95, 128.50, 128.54, 128.81, 141.52, 144.00, 156.20, 170.93, 172.51, 172.88. EI HRMS 529.1973 (M<sup>+</sup> – C<sub>4</sub>H<sub>9</sub>, calcd for C<sub>30</sub>H<sub>29</sub>N<sub>2</sub>O<sub>7</sub> 529.1975).

**N-Acetyl-L-alanyl-D-glutamic Acid,  $\alpha$ -tert-Butyl,  $\gamma$ -Benzyl Diester (11).** A round-bottomed flask was charged with compound **10** (453 mg, 0.772 mmol) and 10% piperidine/CH<sub>2</sub>Cl<sub>2</sub> (22 mL), and the resultant solution was stirred at room temperature for 1 h. The solution was washed with phosphate buffer (pH 5.5, 1 M), water, and brine and then was dried over MgSO<sub>4</sub>. The solvent was removed in vacuo, and the crude residue was redissolved in CH<sub>2</sub>Cl<sub>2</sub> (20 mL). To this solution was added Et<sub>3</sub>N (115  $\mu$ L, 0.849 mmol) and acetic anhydride (80  $\mu$ L, 0.849 mmol), and the resultant mixture was stirred at room temperature overnight. The solvent was removed on a rotary evaporator, and the product was purified by column chromatography (silica gel, 1:4 hexane/EtOAc) to give a colorless oil (314 mg, 100%). <sup>1</sup>H NMR (CDCl<sub>3</sub>):  $\delta$  1.39 (d, 3H, *J* = 7.2 Hz), 1.48 (s, 9H), 1.98–2.54 (m, 7H), 4.46–4.59 (m, 2H), 5.15 (s, 2H), 6.28 (bd, 1H, *J* = 7.2 Hz), 6.94 (bd, 1H, *J* = 7.6 Hz), 7.34–7.41 (m, 5H). <sup>13</sup>C NMR (CDCl<sub>3</sub>):  $\delta$  19.7, 24.3, 28.3, 29.1, 31.4, 49.8, 53.4, 67.7, 83.6, 129.3, 129.4, 129.7, 136.8, 171.1, 171.6, 173.3, 173.8; EI HRMS 350.1476 (M<sup>+</sup> – C<sub>4</sub>H<sub>8</sub>, calcd for C<sub>17</sub>H<sub>22</sub>N<sub>2</sub>O<sub>6</sub> 350.1478).

**N-Acetyl-L-alanyl- $\gamma$ -D-glutamyl( $\alpha$ -O<sup>t</sup>Bu)-L-lysine( $\epsilon$ -N-Boc), Benzyl Ester (13).** A solution of compound **11** (270 mg, 0.664 mmol) in MeOH (20 mL) was charged with Pd/C (5% Degussa type, 32 mg), and the mixture was stirred vigorously under an ambient pressure of

(8) Hardy, L. W.; Kirsch, J. F. *Biochemistry* **1984**, *23*, 1275–1282.

(9) Bulychov, A.; Mobashery, S. *Antimicrob. Agents Chemother.* **1999**, *43*, 1743–1746.

(10) Micetich, R. G.; Singh, R.; Singh, M. P.; Shaw, C. C. *Synthetic Commun.* **1986**, *16*, 453–460.

(11) Patera, A.; Blaszcak, L. C.; Shoichet, B. K. *J. Am. Chem. Soc.* **2000**, *122*, 10504–10512.

hydrogen at room temperature for 3 h. The mixture was then filtered, and the filtrate was concentrated in vacuo to give the crude acid as a white solid (200 mg). <sup>1</sup>H NMR (CDCl<sub>3</sub>): δ 1.37 (d, 3H, *J* = 6.9 Hz), 1.45 (s, 9H), 1.93–2.48 (m, 7H), 4.39–4.66 (m, 2H), 6.81 (bd, 1H, *J* = 7.8 Hz), 7.30 (bd, 1H, *J* = 7.8 Hz). <sup>13</sup>C NMR (CDCl<sub>3</sub>): δ 18.5, 23.0, 26.8, 27.9, 30.1, 48.9, 52.5, 82.5, 170.6, 170.8, 172.7, 176.1. This crude product was redissolved in CH<sub>2</sub>Cl<sub>2</sub>/DMF (12/2 mL), and to this solution was added **12** (256 mg, 0.762 mmol), HOBT (86 mg, 0.635 mmol), and DCC (118 mg, 0.571 mmol). The resultant mixture was stirred at room temperature overnight. Some CHCl<sub>3</sub> (~50 mL) was added to dilute the reaction mixture, and the organic solution was washed with 5% NaHCO<sub>3</sub>, 1 N HCl, water, and brine and then was dried over MgSO<sub>4</sub>. The solvent was removed in vacuo, and the product was purified by column chromatography (silica gel, 50:1 CHCl<sub>3</sub>/MeOH) to give the title compound as a white solid (200 mg, 47%). <sup>1</sup>H NMR (CD<sub>3</sub>OD): δ 1.38 (d, 3H, *J* = 7 Hz), 1.45 (s, 9H), 1.47 (s, 9H), 1.64–2.32 (overlapping s and m, 13H), 3.02–3.06 (m, 2H), 4.20–4.28 (m, 3H), 5.15 (s, 2H), 7.36–7.44 (m, 5H). <sup>13</sup>C NMR (CD<sub>3</sub>OD): δ 16.90, 19.73, 21.63, 24.35, 25.77, 28.30, 28.78, 29.11, 31.43, 39.34, 49.84, 52.27, 53.40, 67.74, 81.03, 83.62, 129.31, 129.44, 129.75, 136.83, 159.01, 171.10, 171.63, 172.89, 173.31, 173.82. Mp 48–50 °C. ESI MS 634.36 (M<sup>+</sup>, calcd for C<sub>32</sub>H<sub>50</sub>N<sub>4</sub>O<sub>9</sub> 634.36).

**Benzhydryl 7β-[N-Acetyl-L-alanyl-γ-D-glutamyl(α-O<sup>t</sup>Bu)-L-lysine-(ε-N-Boc)]-3-acetoxymethyl-3-cephem-carboxylate (15).** To the solution of **13** (200 mg, 0.315 mmol) in MeOH was added Pd/C (5% Degussa, 20 mg), and the mixture was stirred under an ambient pressure of hydrogen at room temperature overnight. The mixture was filtered, and the filtrate was concentrated in vacuo to give the crude acid as a white solid (177 mg). <sup>1</sup>H NMR (CD<sub>3</sub>OD): δ 1.35–1.54 (overlapping s, d, and m, 25H), 1.72–1.23 (overlapping s and m, 6H), 3.05–3.11 (m, 2H), 4.27–4.47 (overlapping bs and m, 4H), 4.95 (bs, 1H), 6.00 (bs, 1H), 7.09 (bs, 1H). This crude product was redissolved in CH<sub>2</sub>Cl<sub>2</sub> (10 mL), and to this solution was added **14** (143 mg, 0.325 mmol), HOBT (44 mg, 0.325 mmol), and DCC (60 mg, 0.292 mmol). The resultant mixture was stirred at room temperature overnight. Some CH<sub>2</sub>Cl<sub>2</sub> (~50 mL) was added to dilute the reaction mixture, and the organic solution was washed with 5% NaHCO<sub>3</sub>, 10% citric acid, water, and brine and then was dried over MgSO<sub>4</sub>. The solvent was removed in vacuo, and the product was purified by column chromatography (silica gel, 2:1 EtOAc/hexane, then 15:1 CH<sub>2</sub>Cl<sub>2</sub>/2-propanol) to give an off white powder (86 mg, 28%). Mp 168–170 °C. <sup>1</sup>H NMR (CD<sub>3</sub>OD): δ 1.36 (d, 3H, *J* = 7 Hz), 1.44 and 1.46 (2 overlapping s, 18H), 1.66–2.33 (overlapping s and m, 16H), 3.02–3.05 (m, 2H), 3.51 (d, 1H, *J* = 18.5 Hz), 3.64 (d, 1H, *J* = 18.5 Hz), 4.23–4.37 (m, 3H), 4.74 (d, 1H, *J* = 13 Hz), 4.96 (d, 1H, *J* = 13 Hz), 5.11 (d, 1H, *J* = 5 Hz), 5.73 (d, 1H, *J* = 5 Hz), 6.91 (s, 1H), 7.25–7.44 (m, 10H). <sup>13</sup>C NMR (CD<sub>3</sub>OD): δ 16.57, 19.34, 20.57, 22.90, 26.59, 27.08, 27.99, 28.27, 28.41, 31.10, 31.91, 40.06, 49.12, 52.43, 52.91, 57.76, 59.80, 64.25, 78.85, 81.24, 83.62, 126.26, 127.41, 127.85, 128.38, 128.51, 128.79, 128.86, 140.18, 140.43, 157.82, 161.61, 171.45, 171.52, 172.59, 173.59, 174.29, 174.34, 174.38, 174.49. FAB MS 965 (M<sup>+</sup> + H, calcd for C<sub>48</sub>H<sub>65</sub>N<sub>6</sub>O<sub>13</sub>S 965).

**7β-[N-Acetyl-L-alanyl-γ-D-glutamyl-L-lysine]-3-acetoxymethyl-3-cephem-carboxylic Acid TFA Salt (6).** A solution of compound **15** (11 mg, 0.0114 mmol) in TFA (1 mL) and anisole (1 drop) was stirred at ice–water temperature for 10 min, at which time the ice–water bath was removed and the stirring was continued for another 20 min. The solvent was removed in vacuo. The product was precipitated from MeOH/ether to give an off-white powder (9 mg, quant.). Mp 167 °C (dec); <sup>1</sup>H NMR (CD<sub>3</sub>OD): δ 1.32–2.05 (overlapping m and s, 16H), 2.22–2.35 (m, 3H), 2.93 (t, 2H, *J* = 7.5 Hz), 3.42 (d, 1H, *J* = 18 Hz), 3.62 (d, 1H, *J* = 18 Hz), 4.31–4.41 (m, 3H), 4.83 (d, 1H, *J* = 13 Hz), 5.04–5.07 (2 overlapping d, 2H), 5.68 (d, 1H, *J* = 4.5 Hz). <sup>13</sup>C NMR (CD<sub>3</sub>OD): δ 16.90, 19.78, 21.63, 22.54, 25.77, 26.75, 27.43, 31.11, 31.66, 39.34, 49.74, 52.27, 53.49, 57.55, 59.33, 63.98, 119.72, 130.28,

**Table 1.** Crystallographic Statistics and Refinement Results

space group	C2
cell constants: (Å), (deg)	<i>a</i> = 118.81, <i>b</i> = 76.30, <i>c</i> = 98.13, <i>β</i> = 116.21
resolution <sup>a</sup> (Å)	25.0–1.71 (1.77–1.71)
total observations	440 555
unique reflections	83 273
<i>R</i> <sub>merge</sub> (%)	4.1 (12.2)
completeness (%)	98.1 (97.0)
<i>I</i> / <i>σ</i> <sub><i>i</i></sub>	32.7 (10.7)
number of protein residues	713
number of water molecules	825
RMSD bond lengths (Å)	0.017
RMSD bond angles (deg)	2.0
average B-factor for protein	12.5
average B-factor for compound <b>6</b>	42.8
average B-factor for solvent	33.0
<i>R</i> -factor (%)	15.4
<i>R</i> <sub>free</sub> <sup>b</sup> (%)	19.1

<sup>a</sup> Values in parentheses are for the highest-resolution shell. <sup>b</sup> *R*<sub>free</sub> was calculated with 5% of the reflections set aside randomly.

164.44, 166.34, 172.36, 172.85, 174.14, 174.20, 174.26, 174.32. ESI MS 643.25 (M<sup>+</sup>, calcd for C<sub>26</sub>H<sub>39</sub>N<sub>6</sub>O<sub>11</sub>S 643.24).

**Crystallization and Data Collection.** Crystals of Q120L/Y150E mutant were grown by seeding techniques. Droplets of 10 μL containing 3.9 mg/mL of the protein in 1.0 M potassium phosphate buffer (pH 8.7) were seeded with microcrystals of WT AmpC and placed over a 1.7 M potassium phosphate buffer well solution, pH 8.7. Crystals appeared within 5–7 days after equilibration at 22 °C and grew to a maximum size of 0.2 × 0.2 × 0.2 mm<sup>3</sup> in a week. Crystals were soaked in a 50 mM solution of compound **6** (1.7 M KP<sub>i</sub>, pH 8.7) for 3 h and then dipped in cryo-protectant solution (50 mM of compound **6** and 20% sucrose in 1.7 M KP<sub>i</sub>, pH 8.7) for 1 min. The crystals were flash-cooled in liquid nitrogen. Diffraction data were collected from a single crystal on the 5ID beamline of DND-CAT at Advance Photon Source (Argonne, IL). Two sets of data, at high and low resolution, were collected at a wavelength of 1.0000 Å using an MARCCD detector. A total of 450 frames were integrated, and 440 555 reflections were scaled and merged using the HKL package.<sup>12</sup> The data are 98.1% complete to 1.71 Å resolution (Table 1). Crystals belong to the space group C2, with two AmpC molecules in the asymmetric unit.

**Structure Solution and Refinement.** The phases were determined by molecular replacement using AmoRe.<sup>13</sup> The best result from the single body solution was fixed in order to find a second monomer in the asymmetric unit. The solution of this run was used as a starting model for rigid body refinement in CNS.<sup>14</sup> After torsion angle simulated annealing and several rounds of Cartesian and B-factor refinement, the model was manually corrected using 2Fo–Fc and Fo–Fc sigma<sub>A</sub>-weighted electron density maps displayed with TURBO.<sup>15</sup> The compound was then fit in the site using Fo–Fc difference electron density. Further refinement in CNS led to *R*<sub>cryst</sub> and *R*<sub>free</sub> values of 17.4 and 19.7%, respectively, for all data to 1.71 Å. At this stage, alternative conformations were added and further refinement was conducted in REFMAC.<sup>16</sup> After several rounds of refinement using TLS parameters<sup>17</sup> and manual corrections, the refinement converged to *R*<sub>cryst</sub> and *R*<sub>free</sub> values of 15.4 and 19.1%, respectively (Table 1).

(12) Otwinowski, Z.; Minor, W. *Methods Enzymol.* **1997**, *276*, 307–326.

(13) Navaza, J. *Acta Crystallogr., Sect. A* **1994**, *50*, 157–163.

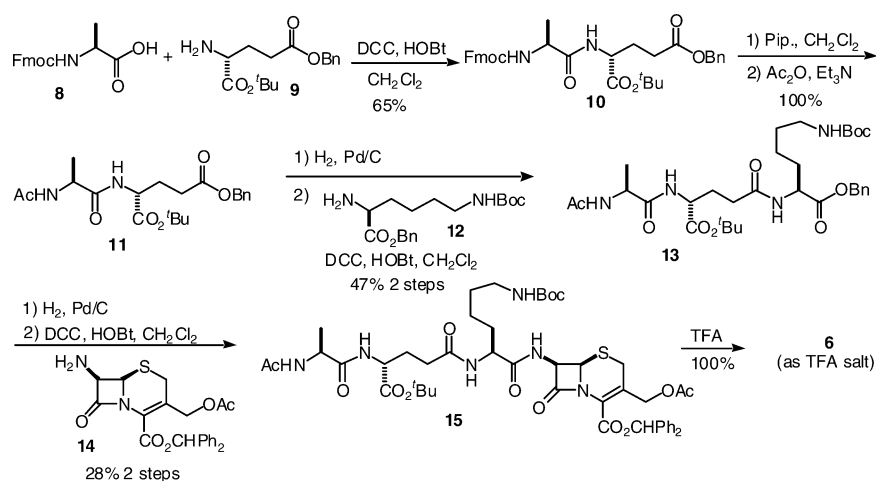
(14) Brünger, A. T.; Adams, P. D.; Clore, G. M.; DeLano, W. L.; Gros, P.; Grosse-Kunstleve, R. W.; Jiang, J. S.; Kuszewski, J.; Nilges, M.; Pannu, N. S.; Read, R. J.; Rice, L. M.; Simonson, T.; Warren, G. L. *Acta Crystallogr., Sect. D* **1998**, *54*, 905–921.

(15) Cambillau, C.; Roussel, A. *Turbo Frodo*, OpenGL Ed. ed.; Universite Aix-Marseille II: Marseille, France, 1997.

(16) Murshudov, G. N.; Lebedev, A.; Vagin, A. A.; Wilson, K. S.; Dodson, E. J. *Acta Crystallogr., Sect. D* **1999**, *55*, 247–255.

(17) Winn, M. D.; Isupov, M. N.; Murshudov, G. N. *Acta Crystallogr., Sect. D* **2001**, *57*, 122–133.

Scheme 1

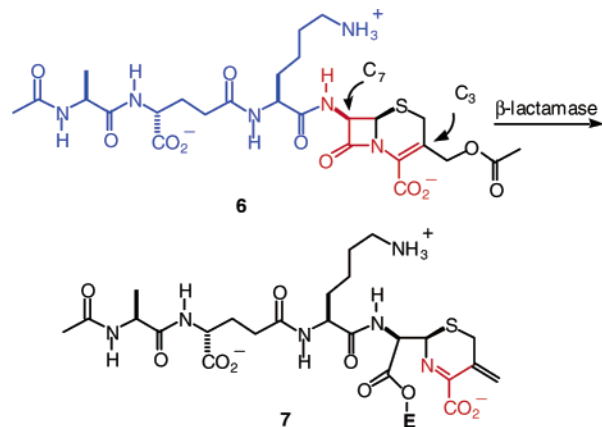


**Computational Procedures.** The X-ray structure of the acyl–enzyme complex provided the initial coordinates for the molecular dynamics simulations. Crystallographic waters were retained, and hydrogen atoms were added to the protein using the “protonate” program, which is part of the AMBER 7<sup>18</sup> suite of programs. AMBER force field parameters and atomic charges were assigned to all atoms using the “parm99” set of parameters. The Sybyl program (Tripos Inc., St. Louis, MO) was used for the manipulation and visualization of all structures and for the protonation of the bound ligand. The atomic charges of the bound ligand were determined using the RESP methodology.<sup>19</sup> This consisted of first optimizing the molecules using the AM1 Hamiltonian, followed by an HF/6-31G\* single-point energy calculation to determine the electrostatic potential around the molecule, which was subsequently used in the two-stage RESP fitting procedure. The Gaussian 98 package<sup>20</sup> was used to carry out all ab initio calculations. The acyl–enzyme complex was immersed in a box of TIP3P<sup>21</sup> water molecules such that no atom in the acyl–enzyme complex was within 12 Å from any side of the box; after solvation of the 5650-atom acyl–enzyme complex, the system consisted of a total of 53 830 atoms. All bonds involving hydrogen atoms were constrained using the SHAKE algorithm, and a 2-fs time step was used. The particle mesh Ewald<sup>22</sup> method was used to treat long-range electrostatics. Water molecules were first energy minimized and equilibrated by running a short simulation with the acyl–enzyme species fixed using Cartesian restraints. This was followed by a series of energy minimizations where the Cartesian restraints were gradually relaxed from 500 kcal/Å<sup>2</sup> to 0 kcal/Å<sup>2</sup> and the system was subsequently slowly heated to 300 K via a 300 ps molecular dynamics run. Another 50 ps simulation was carried

out at 300 K for further equilibration. A 2.6 ns simulation at constant pressure and temperature (1 atm and 300 K, respectively) was then carried out on an in-house beowulf cluster. Snapshots were collected every 0.2 ps.

## Results and Discussion

Cephalosporin **6** was conceived as a probe in exploring the potential surface interactions of peptidoglycan with the class C  $\beta$ -lactamase. The  $\beta$ -lactam nucleus of the cephalosporin mimics the two D-Ala residues of the peptidoglycan (the portions traced in red). The acyl moiety at the C<sub>7</sub> amine (shown in blue) traces most of the remainder of the peptide in the peptidoglycan. The combined red and blue portions of the structure of **6** represent the strand of peptidoglycan that would acylate the active-site serine (i.e., E-OH). Species **7**, in essence, depicts the first peptidoglycan strand that has acylated the active-site serine. On active-site acylation, the “terminal D-Ala residue” from the strand of the peptidoglycan would be eliminated (the portions of **7** shown in red).



Compound **6** was synthesized according to Scheme 1. The tripeptide **13** was constructed by standard peptide coupling procedures. After the removal of the benzyl group from this peptide, it was coupled to cephalosporin **14** to give **15**. A global deprotection by TFA afforded compound **6**.

To explore how compound **6** would be recognized by a class C  $\beta$ -lactamase, the crystal structure of its complex with the Q120L/Y150E mutant of AmpC was determined to 1.71 Å. This mutant is deacylation-deficient,<sup>11</sup> and it allowed us to trap the

- (18) Case, D. A.; Pearlman, D. A.; Caldwell, J. W.; Cheatham, T. E., III; Wang, J.; Ross, W. S.; Simmerling, C. L.; Darden, T. A.; Merz, K. M.; Stanton, R. V.; Cheng, A. L.; Vincent, J. J.; Crowley, M.; Tsui, V.; Gohlke, H.; Radmer, R. J.; Duan, Y.; Pitera, J.; Massova, I.; Seibel, G. L.; Singh, U. C.; Weiner, P. K.; Kollman, P. A. *AMBER*, 7th ed.; University of California: San Francisco, 2002.
- (19) Bayly, C. I.; Cieplak, P.; Cornell, W. D.; Kollman, P. A. *J. Chem. Phys.* **1993**, *97*, 10269.
- (20) Frisch, M. J.; Trucks, G. W.; Schlegel, H. B.; Scuseria, G. E.; Robb, M. A.; Cheeseman, J. R.; Zakrzewski, V. G.; Montgomery, J. A., Jr.; Stratmann, R. E.; Burant, J. C.; Dapprich, S.; Millam, J. M.; Daniels, A. D.; Kudin, K. N.; Strain, M. C.; Farkas, O.; Tomasi, J.; Barone, V.; Cossi, M.; Cammi, R.; Mennucci, B.; Pomelli, C.; Adamo, C.; Clifford, S.; Ochterski, J.; Petersson, G. A.; Ayala, P. Y.; Cui, Q.; Morokuma, K.; Malick, D. K.; Rabuck, A. D.; Raghavachari, K.; Foresman, J. B.; Cioslowski, J.; Ortiz, J. V.; Stefanov, B. B.; Liu, G.; Liashenko, A.; Piskorz, P.; Komaromi, I.; Gomperts, R.; Marti, R. L.; Fox, D. J.; Keith, T.; Al-Laham, M. A.; Peng, C. Y.; Nanayakkara, A.; Gonzalez, C.; Challacombe, M.; Gill, P. M. W.; Johnson, B.; Chen, W.; Wong, M. W.; Andres, J. L.; Gonzalez, C.; Head-Gordon, M.; Replogle, E. S.; Pople, J. A. Gaussian Inc.: Pittsburgh, PA, 1998.
- (21) Jorgensen, W. L.; Chandrasekhar, J.; Madura, J. D.; Impey, R. W.; Klein, M. L. *J. Chem. Phys.* **1983**, *79*, 926–935.
- (22) Darden, T. A.; York, D. M.; Pedersen, L. G. *J. Chem. Phys.* **1993**, *98*, 10089.

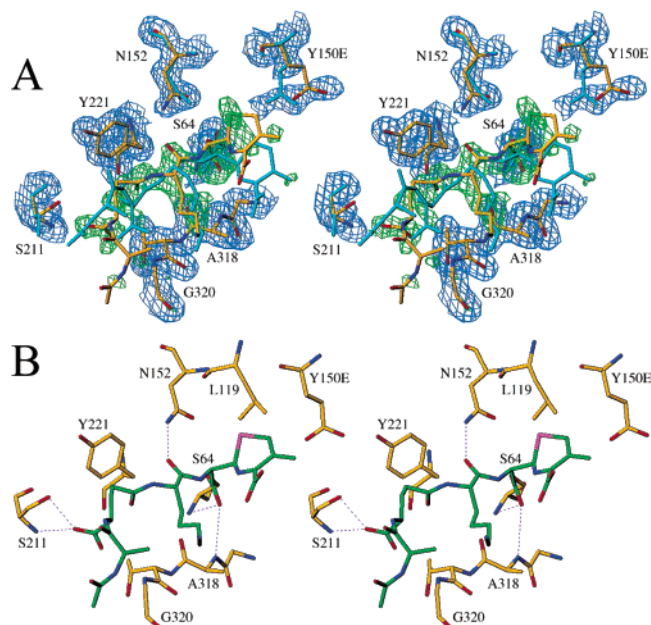


**Figure 1.** Stereoview of the active site of the complex between AmpC and compound **6** (species **7**). (A) Electron density maps of the active site of the monomer B with two alternative conformations of the compound. The 2Fo-Fc sigma<sub>A</sub>-weighted electron density map for protein residues is shown in blue (contoured at 1  $\sigma$ ), and the Fo-Fc omit electron density map for the compound is shown in green (contoured at 2.5  $\sigma$ ). Selected residues of the protein are labeled. One of the alternative conformations is shown colored as follows: carbon in yellow, nitrogen in blue, oxygen in red, and sulfur in green, whereas all atoms of the second conformation are shown in cyan. (B) Hydrogen-bond interactions between selected active-site residues with one of the alternative conformations of the compound (nitrogen in blue, oxygen in red, ligand carbon atoms in green, protein carbon atoms in yellow, and sulfur in magenta).

AmpC/6 complex (species **7**). Evaluation of the structure by Procheck<sup>23</sup> showed that all residues are in the most favored and additionally allowed regions of the Ramachandran plot. The refined model is well fit in 2Fo-Fc electron density, except three residues at positions 284–286 of monomer A, which have disconnected density and were removed from the final model. The two monomers in the structure are very similar, except for this loop region; the overall RMSD is 0.86 Å for all C $\alpha$  atoms and is 0.35 Å with the 280–290 loop omitted.

The electron density in the active sites of both monomers indicates the presence of species **7** covalently bound to the O $\gamma$  of the Ser64. Admittedly, this density is “patchy,” which might indicate low occupancy, multiple ligand conformations, or both. Despite this “patchiness,” there are clear indications that species **7** is present. There is strong electron density for atoms all along the length of species **7**, from the dihydrothiazine sulfur to the ester carbonyl, to the C<sub>7</sub> side-chain amide group and large portions of the distal C<sub>7</sub> peptide, including the lysine moiety. The relatively high resolution of the structure (1.71 Å) allowed us to adopt a combined occupancy and conformation strategy in fitting the ligand to the observed electron density. In monomer A, species **7** is modeled with half occupancy and it shares the same space with several water molecules, also modeled with partial occupancy. In monomer B, the ligand is modeled in two alternative conformations with an occupancy of 0.5 each (Figure 1A). Several side chains of the active site appear to be involved

in correlated movement to accommodate repositioning of species **7** in the active site, and they are also modeled with two alternative conformations. The conformation of the ligand in the active site of monomer A is very similar to one of the alternative conformations of the compound in monomer B (Figure 1A). Species **7** makes several hydrogen bonds with active site residues (Figure 1B). The carbonyl oxygen of the ester moiety is in the “oxyanion” hole, interacting with amide nitrogens of Ser64 and Ala318. The carbonyl oxygen of the lysine in the C<sub>7</sub> side-chain hydrogen bonds with side-chain nitrogen of Asn152. Finally, one of the carboxylate oxygens of the C<sub>7</sub> side-chain hydrogen bonds with the O $\gamma$  and the main-chain nitrogen of Ser211.

An intriguing feature of the complex between AmpC and species **7** was the high degree of movement observed in the ligand, especially in the distal parts of the C<sub>7</sub> side chain. Although movement in the distal regions of ligands has been observed in other AmpC/ligand complexes,<sup>23–25</sup> it was precisely this region of the ligand that was most informative regarding substrate recognition and differences from PBP. We wondered if the movement observed in the crystal structure was in some sense an artifact of crystallography, for instance reflecting disorder in the crystal or problems with trapping in the deacylation-deficient mutant, or whether it represented a true aspect of molecular recognition between the AmpC enzyme and this substrate. To investigate this question, we turned to the molecular dynamics simulation of the AmpC/7 complex.

Molecular dynamics simulations provided insights into the conformational states as a function of time. Over the course of the 2.6 ns of simulation, snapshots were collected and superimposed on the initial X-ray structure. The resulting structures were used to determine the root-mean-square (rms) deviation and atomic fluctuations, which provide a measure of the flexibility for various regions of the protein and ligand.

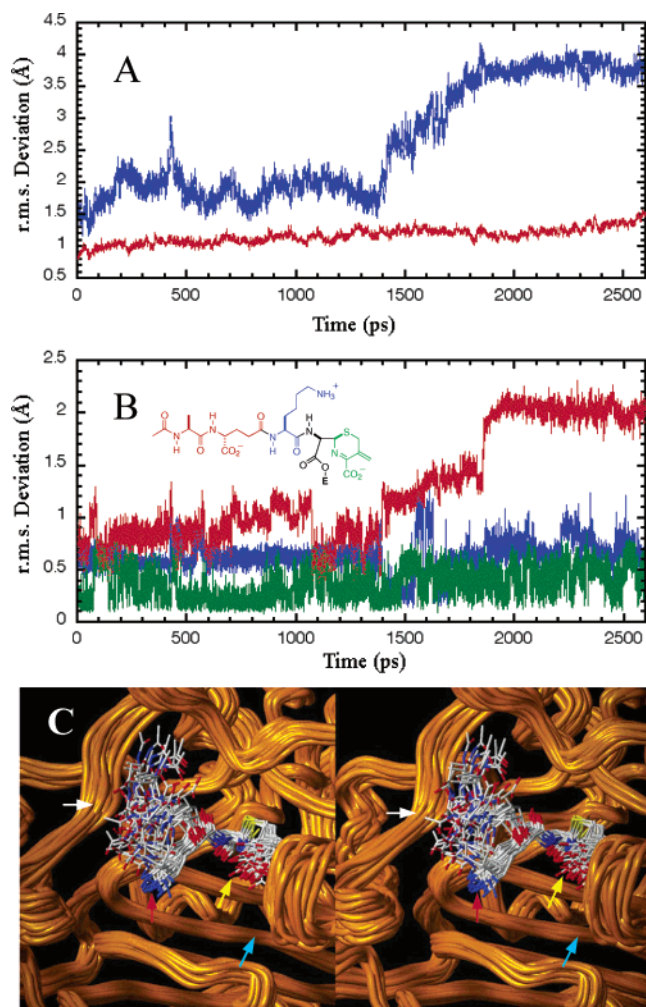
Evolution of the rms deviation with respect to time of the C $\alpha$  atoms of the protein and of species **7** are shown in Figure 2A. The rms deviation of the protein is found not to exceed 1.5 Å, consistent with the crystallographic result of a stable protein structure. The rms deviation value of the ligand, on the other hand, fluctuated around 2 Å for the first 1.4 ns of simulation, which subsequently gradually increased reaching a maximum of 4.2 Å at 1.8 ns. This increase indicates that the ligand is prone to substantial movement in the active site of the protein.

Figure 2B depicts more closely the dynamics of different parts of the ligand. The portion of the ligand highlighted in red was found to be the most mobile, with its rms deviation reaching 2.3 Å, which is more pronounced than the 1.3 and 0.9 Å rms deviations experienced by the lysine (in blue) and the dihydrothiazine ring, highlighted in green. To illustrate the range of movement that the ligand experiences in the active site of the  $\beta$ -lactamase, 26 structures were collected at 100 ps intervals and are shown superimposed in Figure 2C. The L-Ala- $\gamma$ -D-Glu region of the ligand (white arrows in Figure 3C) shows significant movement and samples a wide variety of conformations. At the initial stages of the simulation, the acetyl carbonyl oxygen of the ligand was pointing toward the guanidinium moiety of Arg-201, and the carboxylate moiety of D-Glu was

(23) Lobkovsky, E.; Billings, E. M.; Moews, P. C.; Rahil, J.; Pratt, R. F.; Knox, J. R. *Biochemistry* **1994**, *33*, 6762–6772.

(24) Tondi, D.; Powers, R. A.; Caselli, E.; Negri, M. C.; Blazquez, J.; Costi, M. P.; Shoichet, B. K. *Chem. Biol.* **2001**, *8*, 593–611.

(25) Powers, R. A.; Caselli, E.; Focia, P. J.; Prati, F.; Shoichet, B. K. *Biochemistry* **2001**, *40*, 9207–9214.



**Figure 2.** (A) Root-mean-square (rms) deviation from the X-ray structure of the C $\alpha$  carbon atoms of the protein (red) and non-hydrogen atoms of species **7** (blue). (B) Root-mean-square deviation of different portions of the ligand from the X-ray structure. The inset shows a schematic of species **7** with colors corresponding to the root-mean-square deviations from the plot. (C) A stereoview of the superimposition of 26 snapshots collected from the 2.6 ns simulation at 100 ps intervals. Species **7** is shown in capped-sticks representation and color coded according to atom types (C, N, O, and S are in white, blue, red, and yellow, respectively). The protein backbone is shown as an orange tube. The white arrow points to the L-Ala- $\gamma$ -D-Glu portion of species **7**, while the red and yellow arrows point to lysine and the six-membered ring, respectively. The blue arrow points to the inserted loop specific to class C  $\beta$ -lactamases that prevents binding of the second strand of the peptidoglycan to the active site.

pointing toward Ser-209 (3.9 Å). The orientation of these moieties corresponded to that adopted by conformer **1** (see compound colored according to the atom types in Figure 1A) in its acyl-enzyme complex with AmpC (conformer **1**/AmpC complex X-ray structure was used as the initial structure for the molecular dynamics simulation). As the trajectory progressed, the acetyl moiety gradually flipped over to eventually occupy a large cavity in the active site (12 o'clock in Figure 2C), while the D-Glu carboxylate occupied the initial position of the acetyl moiety to form hydrogen bonding interactions with Arg-201. In the process of flipping, the L-Ala- $\gamma$ -D-Glu moiety adopted similar conformations to those found in conformer **2** (see the species colored in cyan in Figure 1A) of the X-ray structure. The molecular dynamics simulation thus provided a detailed account of the conformational flexibility that the ligand

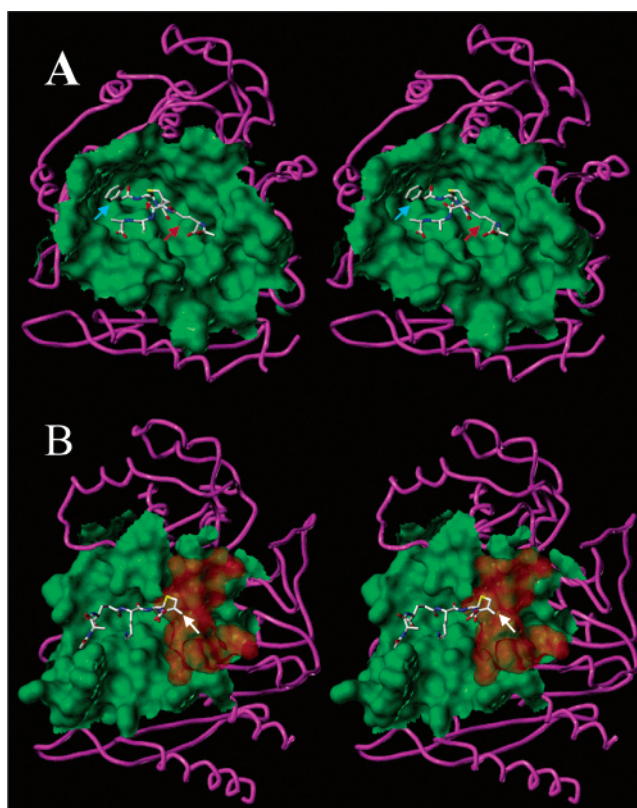


**Figure 3.** (A) Stereoview of the *Streptomyces* R61 DD-carboxypeptidase/transpeptidase acylated by **16**. A water-accessible surface area (shown in green) depicts the active site and species **17** is represented according to atom types (white, blue, red, and yellow correspond to C, N, O, and S, respectively). The blue and red arrows point to the portions of the species **17** colored in blue and red, respectively. (B) Stereoview of AmpC acylated by compound **6** with the water-accessible surface within the active site depicted in green. The ligand is depicted in the capped-stick representation and is colored according to atom types. The white arrow is pointing to the exocyclic methylene of species **7**. A translucent orange/red water-accessible surface was constructed for the inserted peptide spanning residues 285 to 296.

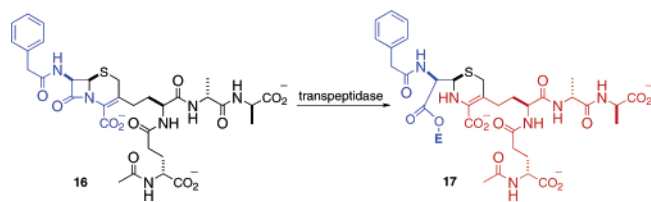
demonstrates within the active site, which includes conformers **1** and **2**, both seen by the X-ray diffraction data. The fact that this portion of the ligand was found to be highly mobile in the molecular dynamics simulation is also consistent with the X-ray diffraction data, which indicated that electron density in that region was such that the structure could not be unambiguously resolved into one conformer.

Movements in the other regions of species **7** were more attenuated, as shown by the rms deviations in Figure 2B and as depicted in Figure 2C. The lysine residue (red arrow, Figure 2C) does not undergo any major conformational change over the course of the trajectory. The ligand ring (yellow arrow in Figure 2C) also does not show any large conformational change, although it is of interest to note that most of the fluctuations occurs near the carboxylate moiety of the ring.

We recently reported the synthesis of compound **16** and its evaluation by X-ray in a complex with a bifunctional DD-transpeptidase/DD-peptidase.<sup>26</sup> The portion in blue of cephalosporin **16** mimics the first strand of peptidoglycan that acylates the active-site serine of the PBP. On enzyme acylation, the portions in blue and red of species **17** represent the two strands

(26) Lee, W.; McDonough, M. A.; Kotra, L.; Li, Z. H.; Silvaggi, N. R.; Takeda, Y.; Kelly, J. A.; Mobashery, S. *Proc. Natl. Acad. Sci. U.S.A.* **2001**, *98*, 1427–1431.

of peptidoglycan poised for the formation of the “cross-linked” cell wall. The 1.2 Å X-ray structure for this complex from the Kelly laboratory provided the first glimpse of how DD-transpeptidases may organize two strands of the bacterial peptidoglycan in their active sites en route to cross-linking. Figure 3A shows an image of the high-resolution structure of this complex, with the active site depicted as a Connolly surface (in green). To the right of the active site, it is open to accommodate the second strand of the peptidoglycan and the “wall” at 11 o’clock is the surface for interactions of the first peptidoglycan. The same perspective is shown for the complex of species **7** within the active site of AmpC  $\beta$ -lactamase in Figure 3B, as reported in this manuscript. It is noteworthy that the “wall” for interactions with the first strand of the peptidoglycan is entirely absent in the  $\beta$ -lactamase complex. This gives a simple structural perspective for why the crystallographic data and dynamics simulations could not fix the “first strand of peptidoglycan” in species **7** in an effective binding geometry, as the enzyme surface here has evolved away from such binding ability. It is also revealing that the insertion of the peptide within the active site at 3 o’clock (shown as a translucent orange/red water-accessible surface in Figure 3B; pointed to by the blue arrow in Figure 2C) clearly has abolished the ability of a second strand of the peptidoglycan to bind to this subsite. This inserted peptide is not known to play any catalytic role in the reaction of the  $\beta$ -lactamase. The exocyclic methylene group of the six-membered ring in species **7** is flush against the side of the insertion peptide (white arrow in Figure 3B), and there is no room for a larger ligand such as species **17**, seen in the active site of the PBP. These two crystallographic images provide evidence for the structural reasons behind the lack of recognition of the peptidoglycan by at least class C  $\beta$ -lactamases, which must have paved the way for the emergence of a highly competent catalyst in the destruction of  $\beta$ -lactam antibiotics in resistant bacteria.



**Concluding Remarks.** Because of the kinship of  $\beta$ -lactamases and PBPs, much effort has been dedicated to demonstrating that they could potentially carry out each other’s reaction(s). This has not been an easy task, although there exist evidence that some DD-peptidases can hydrolyze  $\beta$ -lactam antibiotics<sup>27–29</sup> and some  $\beta$ -lactamases have marginal peptidase activities.<sup>30</sup> *From the present report, it would appear that at least class C  $\beta$ -lactamases have fully divested from the ability to recognize the peptidoglycan.* In essence, the utility of cephalosporin **6** was in the fact that it acylates the active-site serine, forcing sequestration of the “peptidoglycan strand” (i.e., the C<sub>7</sub> substituent) into the active site. Despite this forced coexistence within the complex, binding of the surrogate for the peptidoglycan is not stabilized by the protein. The requisite surface for the interaction with the peptidoglycan that acylates the active site serine in PBPs no longer exists in the  $\beta$ -lactamase active site. Similarly, the peptide insertion within the active site of  $\beta$ -lactamase abolishes the potential binding site for the second peptidoglycan in the active site, such as it is in DD-transpeptidases. The X-ray structure for the cephalosporin ligand indicates at least two binding modes. Molecular dynamics simulations showed that the ligand samples a substantial conformational space, which incidentally included the two species seen in the X-ray structure. The evidence presented here provides structural insight into how this antibiotic resistance enzyme has divested itself from interaction with the substrate for the parental enzymes, en route to achieving full catalytic effectiveness in its intended function in living bacteria.

**Acknowledgment.** This work was supported by Grants AI33170 and GM61629 (to S.M.) and by GM63815 (to B.K.S.) from the National Institutes of Health. We thank Alexandera Patera for assistance with initial crystallography and for protein expression. The X-ray crystal structure of compound **6** in complex with the mutant AmpC has been deposited with the PDB, accession number 1O07.

JA034861U

- (27) Davies, C.; White, S. W.; Nicholas, R. A. *J. Biol. Chem.* **2001**, *276*, 616–623.  
 (28) Livermore, D. M. *J. Antimicrob. Chemother.* **1987**, *19*, 733–742.  
 (29) Deka, R. K.; Machius, M.; Norgard, M. V.; Tomchick, D. R. *J. Biol. Chem.* **2002**, *277*, 41857–41864.  
 (30) Rhazi, N.; Galleni, M.; Page, M. I.; Frere, J. M. *Biochem. J.* **1999**, *341* (Pt 2), 409–413.